

A new atmospheric background state to diagnose local waveguidability

Christopher Polster¹ and Volkmar Wirth¹

¹Institute for Atmospheric Physics

December 19, 2023

Abstract

A new procedure to obtain a longitudinally varying and slowly evolving atmospheric background state for the analysis of Rossby waveguides is described and discussed. The procedure is a rolling zonalization scheme, redistributing Ertel potential vorticity in a moving window to separate waves from the background. Waveguides are subsequently diagnosed from the gradient of the logarithm of potential vorticity. The effectiveness of the wave-background separation, even in large-amplitude conditions, is illustrated with reanalysis data. Established climatological mean waveguide structures are recovered from the rolling-zonalized state in the limit of long-term aggregation. Two contrasting episodes of Rossby wave packet propagation demonstrate how the evolution of waveguides derived from rolling zonalization can correspond to the development of superposed wave packets. The ability of the procedure to work with snapshots of the atmosphere provides new opportunities for waveguide research.

A new atmospheric background state to diagnose local waveguidability

Christopher Polster¹ and Volkmar Wirth¹

¹Institute for Atmospheric Physics, Johannes Gutenberg University, Mainz, Germany

Key Points:

- We construct a new atmospheric background state that is local in both space and time.
- Waveguide information can be extracted from the background state potential vorticity field.
- Our scheme enables instantaneous waveguide analysis while also reproducing established waveguide patterns after long-term aggregation.

Corresponding author: Christopher Polster, cpolster@uni-mainz.de

Abstract

A new procedure to obtain a longitudinally varying and slowly evolving atmospheric background state for the analysis of Rossby waveguides is described and discussed. The procedure is a rolling zonalization scheme, redistributing Ertel potential vorticity in a moving window to separate waves from the background. Waveguides are subsequently diagnosed from the gradient of the logarithm of potential vorticity. The effectiveness of the wave-background separation, even in large-amplitude conditions, is illustrated with reanalysis data. Established climatological mean waveguide structures are recovered from the rolling-zonalized state in the limit of long-term aggregation. Two contrasting episodes of Rossby wave packet propagation demonstrate how the evolution of waveguides derived from rolling zonalization can correspond to the development of superposed wave packets. The ability of the procedure to work with snapshots of the atmosphere provides new opportunities for waveguide research.

Plain Language Summary

Rossby waves are meridional excursions of the jet stream, a strong band of wind in the extratropics. Stationary Rossby waves can cause extreme weather at the surface and travelling waves connect the weather of remote regions on the globe. Paths along which Rossby waves preferentially develop and travel are called waveguides. To detect the presence of a waveguide in atmospheric data, the waves have to be separated from their guiding atmospheric background state first. We introduce a new separation procedure for snapshots of the atmosphere that results in a slowly evolving and longitudinally varying background state. Our background state is a new source of local waveguide information, particularly in applications where no reliable information was available previously.

1 Introduction

Waveguides are paths in the atmosphere along which Rossby wave activity is preferentially ducted (Branstator, 1983; Hoskins & Ambrizzi, 1993; Chang & Yu, 1999; Martius et al., 2010; Wirth et al., 2018). The concept of a waveguide is important for understanding teleconnection patterns facilitated by Rossby waves (Hoskins & Karoly, 1981; Hsu & Lin, 1992; Branstator, 2002; Branstator & Teng, 2017), the steering of weather systems (Chang et al., 2002), the onset of atmospheric blocking (Nakamura & Huang, 2018), extreme weather (Petoukhov et al., 2013; Kornhuber et al., 2017; White et al., 2021; Rousi et al., 2022) and sub-seasonal to seasonal weather prediction (Hoskins, 2013; Davies, 2015). In this work, we focus on the horizontal propagation of Rossby waves along the extratropical jet waveguide.

Strong and narrow jet streams are known to constitute good Rossby waveguides in the atmosphere (Manola et al., 2013; Harvey et al., 2016; Wirth, 2020). In practice, jet detection schemes (e.g. Spensberger et al., 2017) and jet-associated enhanced gradients of potential vorticity (e.g. Schwierz et al., 2004; Martius et al., 2010; Röthlisberger et al., 2016) are used to extract waveguide information from atmospheric data. Waveguides are diagnosed in barotropic analysis by tracing Rossby waves as rays refracted by the stationary wavenumber field (Karoly, 1983; Hoskins & Ambrizzi, 1993; Ambrizzi et al., 1995), though concerns about the underlying assumptions of the theory have been raised since its inception (Hoskins & Karoly, 1981; Teng & Branstator, 2019; Wirth, 2020). Figure 1 illustrates the general agreement of common diagnostic fields regarding the mean climatological waveguide patterns.

The conceptual picture considers waveguides as features of a wave-free background state onto which waves are superposed. Separating waves and background in the atmosphere post factum is a challenging and not well defined problem, as the scale of both

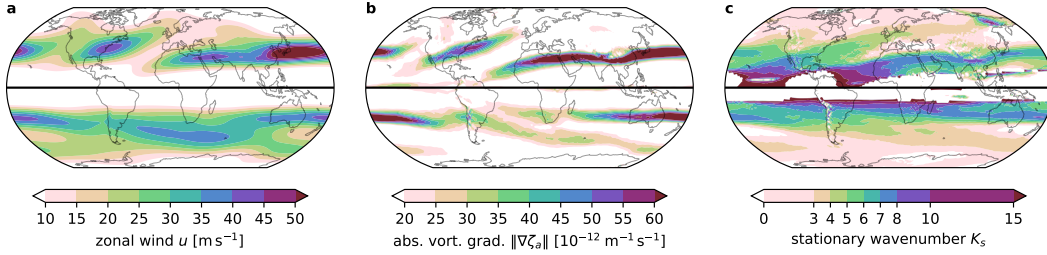


Figure 1. Barotropic waveguide diagnostic fields computed from the 1979–2022 ERA5 winter-mean horizontal wind fields on the 330 K isentrope. (a) zonal wind component u . (b) magnitude of the gradient of absolute vorticity ζ_a . (c) stationary zonal wavenumber K_s , with $K_s^2 = a \cos(\phi)^2 u^{-1} \partial_\phi \zeta_a$ (see text for symbols) and imaginary values plotted white. In general, Rossby waves are expected to propagate preferentially along maxima of these fields. Both hemispheres show winter, i.e. DJF on the northern and JJA on the southern hemisphere.

61 can overlap in time and space (Branstator & Teng, 2017; Wirth & Polster, 2021). Tem-
 62 poral and spatial filters are nevertheless often applied in practice, supported, e.g., by the
 63 finding that waveguides diagnosed from long-term means reflect the known large-scale
 64 teleconnection patterns and storm track regions (Figure 1). However, closer examina-
 65 tion reveals representativity issues due to approximations such as zonally symmetric back-
 66 ground states (Branstator, 1983; Borges & Sardeshmukh, 1995; Branstator, 2002; Hoskins
 67 & Ambrizzi, 1993) and internal variability (Spensberger et al., 2017) and the possibil-
 68 ity of artifacts introduced by inadequate wave-background separation (Dritschel & Scott,
 69 2011; Wirth & Polster, 2021). A separation scheme local in both time and space and resis-
 70 tant to producing artifacts in large-amplitude conditions has not been established so
 71 far.

72 The objective of the present work is to introduce a localized zonalization scheme
 73 as a novel method to compute a background state from a snapshot of the atmosphere
 74 for the purpose of waveguide analysis. Our scheme is both an extension and approxima-
 75 tion of the computation of the modified Lagrangian mean state of Nakamura and Solomon
 76 (2011) and Methven and Berrisford (2015), adding longitudinal variability by means of
 77 a rolling window. Section 2 elaborates on the construction of our procedure and the used
 78 waveguide diagnostic. A background state is then computed from a reanalysis dataset
 79 (section 3) and evaluated regarding its use as a basis for waveguide analysis in section
 80 4. We conclude with a summary and discussion in section 5.

81 2 Methods

82 2.1 Zonalization

83 Zonalization is a conservative rearrangement of potential vorticity (PV), such that
 84 the values of the resulting zonally symmetric PV profile are in descending order from North
 85 to South (Nakamura & Zhu, 2010). We zonalize Ertel PV, in isentropic coordinates given
 86 by $q = \frac{\zeta_a}{\sigma}$, the quotient of absolute vorticity ζ_a and isentropic density $\sigma = -\frac{1}{g} \frac{\partial p}{\partial \theta}$, with
 87 potential temperature θ , pressure p and gravitational acceleration g . The equivalent lati-
 88 tude ϕ_{eq} of a PV contour Q (Butchart & Remsberg, 1986; Allen & Nakamura, 2003) is
 89 implicitly defined as

$$\int_{q \geq Q} \sigma \, dS = \int_{\phi \geq \phi_{\text{eq}}} \sigma_{\text{ref}} \, dS, \quad (1)$$

90 where both integrals are surface integrals evaluated on an isentrope and ϕ is latitude.
 91 The background state isentropic density σ_{ref} must be prescribed for the computation.

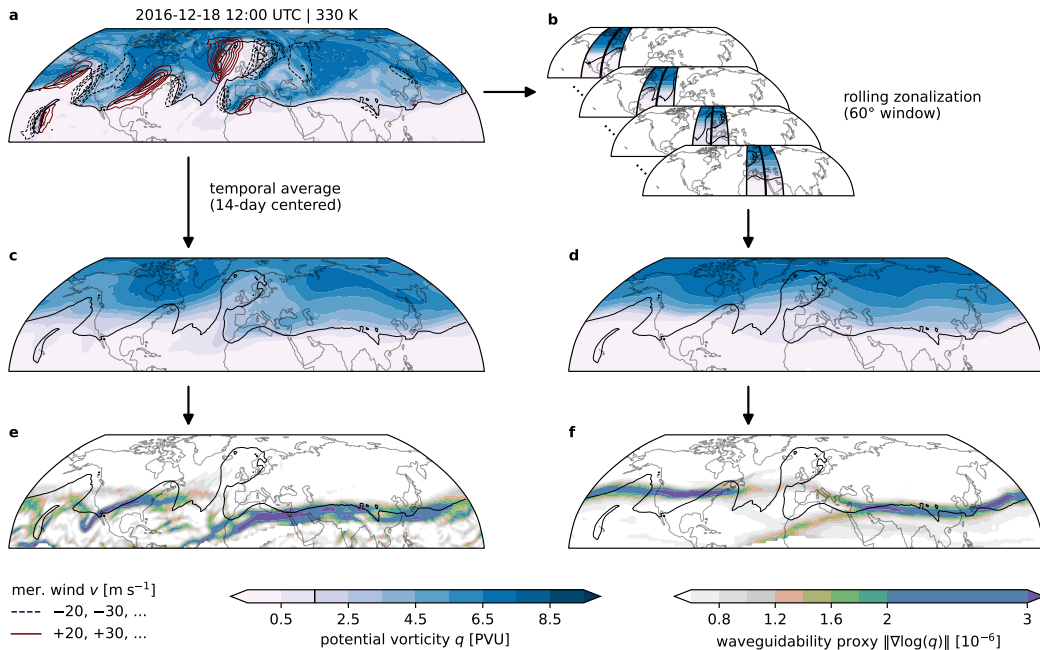


Figure 2. Comparison of time-mean and rolling-zonalized background states on the 330 K isentrope. (a) PV (filled contours) and meridional wind (red and black dashed contours) on 18 December 2016 1200 UTC. For convenience, the 1.5 PVU contour of PV is shown in all panels (solid black). (b) Rolling zonalization illustrated by four individual zonalizations for 90°W, 50°W, 10°W and 30°E. Each window’s central longitude is highlighted in bold. (c) 14 day-mean PV. (d) Rolling-zonalized PV. (e,f) $\|\nabla \log(q)\|$ as a waveguide diagnostic, based on (c) and (d), respectively.

92 In this work, we evaluate relation (1) in a rolling fashion along longitude, using a 60°-
 93 wide window, to obtain a longitudinally varying zonalized state. The zonalized PV
 94 profile is determined for every window position based on the equivalent latitudes of a set
 95 of PV contours and assigned to the central longitude of the window (Figure 2b). We call
 96 this procedure rolling zonalization and the resulting field of zonalized PV profiles (Fig-
 97 ure 2d) a rolling-zonalized background state.

98 Rolling zonalization can be adjusted to the needs of different applications by se-
 99 lecting different window widths, but the choice of this parameter also introduces sub-
 100 jectivity. For the purpose of waveguide detection, we have found results to be robust in
 101 the range of window widths from 60° to 90° and have chosen 60° as our default here. To
 102 be sure, the addition of longitudinal variation invalidates many theoretical results de-
 103 rived for the hemispherically zonalized state (Nakamura & Solomon, 2011; Methven &
 104 Berrisford, 2015; Ghinassi et al., 2020). We do not attempt to recover localized versions
 105 of these theorems in this work. We only note that a localized zonalized state can also
 106 change due to zonal rearrangement of PV in contrast to a hemispherically zonalized state
 107 which can exclusively change due to non-conservative processes.

108 The process of applying zonalization in a rolling fashion does not guarantee that
 109 PV is globally conserved, even though each individual zonalization is conservative. The
 110 loss of exact PV conservation is one of multiple approximations made to facilitate a sim-
 111 ple and practical implementation of our procedure. A significant departure from the ELIPVI
 112 zonalization scheme of Methven and Berrisford (2015) is the omission of PV inversion

113 and an iteration to a consistent background isentropic density field. Instead, we prescribe
 114 σ_{ref} based on a longitudinally rolling mean of σ using the same window width as the zon-
 115 alization. The lack of PV inversion also means that other “byproducts” like the back-
 116 ground state wind are not computed in our approximation. A three-dimensional hemi-
 117 spheric PV inversion required for a localized ELIPVI implementation presents a signif-
 118 icant technical challenge. For practical reasons and accessibility we do not want to in-
 119 cur the substantial computational costs of an inversion-based procedure. By contrast,
 120 a rolling zonalization can be computed in about 100 ms on a single CPU core.

121 2.2 Waveguide Diagnostic

122 We diagnose waveguidability, a non-binary assessment of the propensity of the at-
 123 mosphere to duct Rossby waves (Manola et al., 2013; Wirth, 2020), based on the gra-
 124 dient of the logarithm of the background state PV obtained from the rolling zonaliza-
 125 tion. An example of this field is shown in Figure 2f. To first order, $\|\nabla \log(q)\|$ is propor-
 126 tional to the curvature of the flow $\nabla^2 u$ and thus related to the dispersion relation of Rossby
 127 waves (Martius et al., 2010; Bukenberger et al., 2023). We aim to avoid issues associ-
 128 ated with strong variations of stratification when deriving the location of waveguides from
 129 $\|\nabla \log(q)\|$ (Bukenberger et al., 2023) with the rolling mean-smoothed σ_{ref} . Regions where
 130 $|q| < 0.1 \text{ PVU}$ ($1 \text{ PVU} = 10^{-6} \text{ K m}^2 \text{ kg}^{-1} \text{ s}^{-1}$) are excluded in our waveguide analysis
 131 to avoid the divergence of the logarithm when $q \rightarrow 0$. As a simple criterion for the pres-
 132 ence of a waveguide, we require $\|\nabla \log(|q|)\| > 1.2 \times 10^{-6}$, with q in PVU. We have
 133 verified that our results are not sensitive to the choice of this threshold.

134 3 Data

135 We process ERA5 (Hersbach et al., 2020, 2023) reanalysis fields of u , v and T from
 136 1979 to 2022 (6-hourly). The input fields are obtained with 1.5° horizontal resolution on
 137 18 pressure levels (50 to 850 hPa in steps of 50 hPa; 70 hPa additionally). We compute
 138 potential temperature and isentropic density on pressure levels, then interpolate to isen-
 139 tropes. Vorticity is computed from the interpolated winds and combined with the inter-
 140 polated isentropic density to calculate PV. Surface integrals for the zonalization are eval-
 141 uated with a conditional boxcounting quadrature scheme with regions outside the input
 142 data range omitted. We zonalize each hemisphere separately.

143 4 Results

144 4.1 A First Look

145 We take a first look at a rolling-zonalized state in Figure 2d. The selected date is
 146 from a European blocking event in December 2016 (Maddison et al., 2019; Polster & Wirth,
 147 2023). The rolling-zonalized PV exhibits a wavenumber 2 to 3 pattern in the midlati-
 148 tudes. The meridional spacing of background state PV contours widens locally over west-
 149 ern Europe and resembles an often assumed background state configuration of scale in-
 150 teraction models of atmospheric blocking (Luo et al., 2023). The associated weakened
 151 gradient of PV is reflected in our waveguide diagnostic field (Figure 2f). With a thresh-
 152 old of 1.2×10^{-6} , we detect an interruption of the waveguide in the blocking region, while
 153 a strong and continuous waveguide is found over subtropical Asia and the midlatitude
 154 Pacific and North American regions. Interestingly, our scheme detects strong waveguid-
 155 ability over Asia despite no wave being present there.

156 Comparing the rolling-zonalized (Figure 2d) and the 14-day temporally averaged
 157 PV fields (Figure 2c), we find some common features but also important differences in
 158 the details. Generally, magnitudes of log-PV gradients are similar and the interruption
 159 of the waveguide at the blocking is found in both background states. The temporally av-
 160 eraged PV is also dominated by a wavenumber 2 to 3 structure. However, meridional

PV profiles in the temporally averaged field are non-monotonic and contour overturning at the block location indicates a failure of the temporal average to remove a stationary, large-amplitude eddy. A higher degree of small scale structure in the temporally averaged state translates to considerably noisier waveguides in the associated $\|\nabla \log(q)\|$ field (Figure 2e). The remains of synoptic-scale troughs are visible over the North Pacific and the Asian subtropical waveguide starts further west without a connecting arm from western Europe. In the rolling-zonalized state, the latitude of the waveguide over North America corresponds better to the central latitude of the superposed wave packet than in the time-averaged state.

4.2 Filtering Properties

The temporal evolution of a hemispherically zonalized state is known to be inherently slow (Nakamura & Solomon, 2011; Methven & Berrisford, 2015). Figure 2 suggests that rolling zonalization can produce fields with a broadly similar structure compared to those produced by a temporal filter, despite only using instantaneous data. In an analysis of 44 years of 6-hourly rolling-zonalized PV based on autocorrelation and spectral decomposition we found that the rolling-zonalized background state also evolves inherently slowly, although the characteristics of the temporal behaviour do not correspond directly to that of any simple temporal filter we compared against (not shown).

A rolling-zonalized state (60° window) cuts off virtually all contributions of waves with wavenumbers equal to or larger than 5 in the zonal wavenumber power spectrum of PV (Figure 3a). Wavenumbers 1, 2 and 3 contribute almost all spectral power in the Northern Hemisphere midlatitudes, with only minor contributions from wavenumber 4. We consider the rolling-zonalized state therefore to be free of synoptic- and smaller-scale eddies. Widening the window of the rolling zonalization to 90° reduces the power in wavenumbers 2 to 4 significantly and moves the cut-off wavelength to $k = 4$. By comparison, a 14-day rolling mean still has as much power in wavenumber 6 than the 60° rolling-zonalized state in wavenumber 4 and correlates more strongly with the spectrum of the original PV. In the spectral comparison of Figure 3a, the 60° rolling-zonalized state is closest to the climatological mean state. Similar to the temporal filtering, the spatial filtering properties of rolling zonalization are generally not unlike, but in details importantly different to those of simple averaging procedures.

4.3 Climatological Waveguide Occurrence

Using the 1.2×10^{-6} threshold, we compute the gridpoint-wise occurrence frequency of waveguides in the rolling-zonalized state. Figure 3b shows the winter-time waveguide occurrence for our default window with of 60° longitude on 330 K. Frequent occurrence of an Asian subtropical waveguide extending into the Pacific and a North American/North Atlantic waveguide can be identified on the Northern Hemisphere. On the Southern Hemisphere, a band of more than 40% waveguide occurrence extends around the globe in the midlatitudes with waveguides occurring preferentially in the Pacific sector from Australia to South America. Figure 3c shows the same analysis for a 90°-wide window, resulting in more zonally elongated waveguide occurrence features. The identity of the North Atlantic waveguide as a feature separate from the North Pacific waveguide is less pronounced but differences between the window widths are otherwise small.

We compare the climatological mean barotropic waveguide diagnostic fields in Figure 1 with the waveguide occurrence frequency field in Figure 3b. The climatological mean winter waveguide structure is broadly reproduced in the long-term aggregated waveguide information from individual snapshots of the rolling-zonalized atmosphere. Relative signal strengths of co-located features in Figure 1 and Figure 3b are similar. However, the waveguide signal associated with the North Atlantic jet does not extend as far towards Europe in the frequency field of the rolling-zonalized state and a secondary wave-

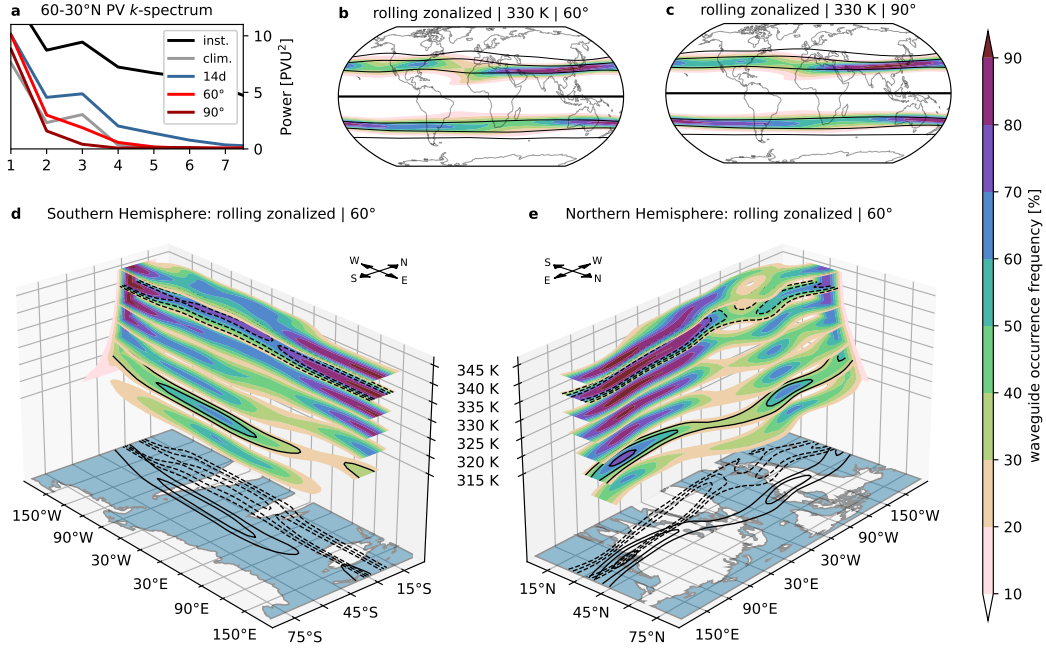


Figure 3. (a) Zonal Wavenumber spectra of instantaneous PV (black), climatological-mean PV (gray), 14 day-rolling-averaged PV (blue) and 60°- (light red) and 90°-window (dark red) rolling-zonalized PV. All spectra of winter months only, spectral power averaged from 60 to 30°N on 330 K. (b,c) Climatological waveguide occurrence on 330 K during winter, derived from a rolling-zonalized state with a 1.2×10^{-6} waveguide detection threshold. Mean contours of rolling-zonalized PV are shown in black. Comparison of 60° (b) and 90° (c) window widths. (d,e) Waveguide occurrence as in (b) but for isentropic levels from 315 to 345 K in steps of 5 K in a 3D visualization for each hemisphere. Selected contours from the 320 (solid) and 340 K (dashed) isentropic levels are reproduced on the bottom maps for orientation. Note that the actual surface of the planet is not a surface of constant potential temperature as depicted here.

211 uide over the Atlantic and Indian Ocean on the Southern Hemisphere is missing. Dif-
 212 ferences in the waveguide features can be contextualized with the vertical structure of
 213 waveguide occurrence in Figure 3d and e. The vertical structure shows the distinct iden-
 214 tities of the North Atlantic and Asian/Pacific waveguides on the Northern Hemisphere
 215 more clearly than 330 K alone. The midlatitude waveguides over the North and South
 216 Atlantic oceans are primarily found on lower isentropic levels than 330 K, while the sub-
 217 tropical waveguides are found at higher levels (Martius et al., 2010; Martin, 2021).

218 4.4 Two Contrasting Episodes

219 We use a refined Hovmöller diagram (Martius et al., 2006) to further illuminate the
 220 waveguide evolution around the December 2016 blocking episode introduced in section
 221 4.1 and Figure 2. Note that the generation of such contour-following Hovmöller diagrams
 222 is particularly easy in the rolling-zonalized state as each PV contour intersects a merid-
 223 ian at most once by construction. Figure 4c shows the evolution of $\|\nabla \log(q)\|$, our waveg-
 224 uidability metric, along the 1.5 PVU contour on 330 K for the 2016 episode. In the snap-
 225 shot for 15 December (Figure 4b), a Rossby wave packet (RWP) stretches from North
 226 America across the North Atlantic into northern Europe, superposed onto a strong waveg-
 227 uide over North America. The waveguide is weaker over the Atlantic with a connection

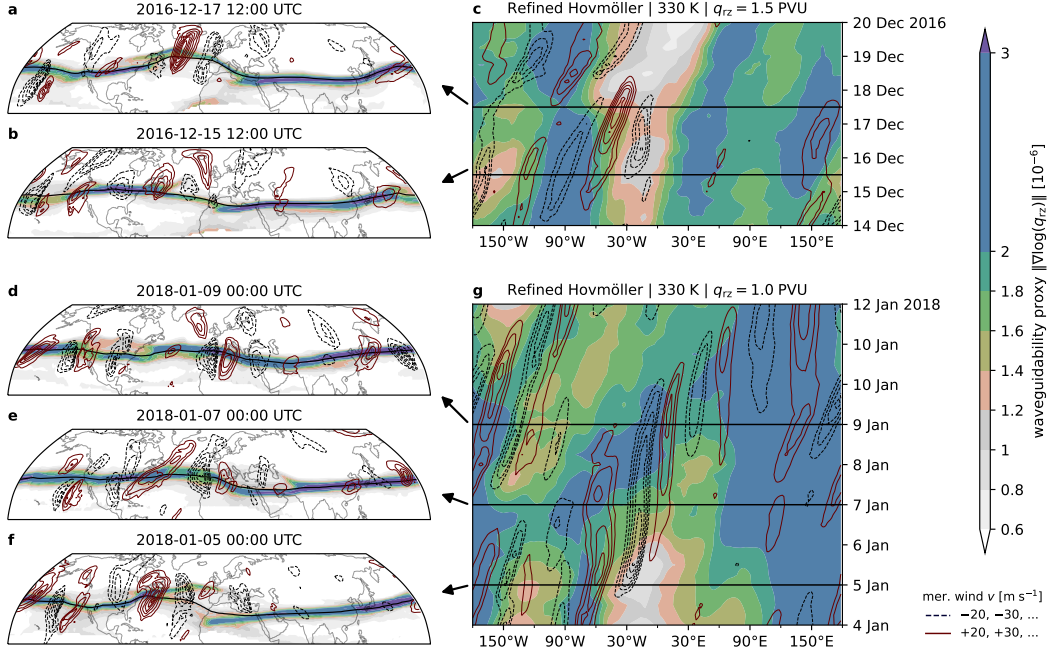


Figure 4. (a,b) $\|\nabla \log(q)\|$ waveguidability diagnostic (filled contours), 1.5 PVU contour of rolling-zonalized PV (black) and meridional wind (dark red/blue contours, in steps of 10 m s^{-1} starting from $\pm 20 \text{ m s}^{-1}$) on 330 K for 17 and 15 December 2016 1200 UTC, respectively. (c) refined Hovmöller diagram of the grad-log-PV waveguide diagnostic (filled contours) and meridional wind (contours). Data is extracted with a 7.5° boxcar smoothing kernel along the contour of 1.5 PVU. (d,e,f) Like (a) but for 9, 7 and 5 December 2018, respectively, and with a PV contour of 1 PVU. (g) Like (c) but for 4 to 12 December 2018 and 1 PVU.

228 to the subtropical waveguide over Asia and a second short branch pointing towards north-
 229 ern Europe. Over the next two days the waveguide strengthens over the Atlantic while
 230 shifting northward together with the 1.5 PVU contour (Figure 4a). A day later, the wave-
 231 guide is interrupted (c.f. Figure 2f) and the propagation of the RWP ceases as the block
 232 has been established (Polster & Wirth, 2023), with low waveguidability dominating the
 233 sector after 17 December (Figure 4c).

234 A different evolution of waveguide and wave is seen in an episode from January 2018
 235 (Figure 4d–g). On 5 January (Figure 4f), a North Atlantic waveguide ends about 20°
 236 further north than a subtropical waveguide over Africa starts, with no significant con-
 237 nection between both. A Rossby wave packet stretches across the Atlantic along the wave-
 238 guide. Strong meridional winds develop over the North Atlantic but the wave packet does
 239 not propagate through the African/European region at first. During 6 January, the two
 240 waveguides connect over the Mediterranean (Figure 4e,g) and a wave signal emerges in
 241 the subtropics at the same time. By 9 January, a strong waveguide has been established
 242 from the North Atlantic across Asia to the North Pacific (Figure 4d). The evolution of
 243 the wave packet appears to occur along this waveguide, with new meridional wind ex-
 244 tremata developing over the Arabian peninsula and further downstream in the following
 245 days (Figure 4g).

246 The two episodes exhibit opposite RWP propagation characteristics in the African/European
 247 region. While the incoming RWP in December 2016 develops into a block with no down-
 248 stream development over Asia, the wave packet in January 2018 continues development

249 along the subtropical waveguide (akin to the equatorward wave energy transfer described
250 by Martius et al., 2010). The parallel evolutions of the midlatitude and subtropical waveg-
251 uides in these two episodes reflect these (non-)propagation patterns: the waveguides are
252 effectively disconnected during the 2016 episode, while the waveguides connect in 2018.

253 5 Summary and Discussion

254 We have introduced a new procedure, rolling zonalization, to compute a three-dimensional
255 background state of the atmosphere that evolves with time. The procedure consists of
256 a rearrangement of potential vorticity in a longitudinally rolling sector on a hemisphere,
257 based on the concept of equivalent latitude. Rolling zonalization combines aspects of both
258 a spatial and a temporal filter. Synoptic-scale eddies of arbitrary amplitude are elim-
259 inated effectively by the zonalization. The resulting background state is slowly evolv-
260 ing even though no information other than the instantaneous state of the atmosphere
261 is required to compute it.

262 Localizing zonalization with a rolling window is straightforward, but it is only an
263 approximation of a scheme consistent with the underlying formalism. We do not com-
264 pute consistent background fields of isentropic density or wind and strict PV conserva-
265 tion is not guaranteed, although we have observed good PV conservation for our setup.
266 We leave the formulation of a theory of wave-mean flow interaction that accomodates
267 our localized zonalized background state to future work. Our present objective is to ad-
268 vance the state of practical application.

269 Using the log-PV gradient of the rolling-zonalized background state as a waveg-
270 uide diagnostic, we were able to recover the established structure of the winter-time cli-
271 matological waveguides in the extratropics. The aggregation of instantaneous waveguide
272 information into a frequency-based perspective on waveguide occurrence complements
273 earlier climatological mean-based results (see also White, 2019). Two contrasting episodes
274 of Rossby wave packet propagation demonstrated how the zonalization-derived waveg-
275 uides can correspond to the local development of superposed wave trains. An interrupted
276 waveguide in the first episode coincided with the onset of a block. A connected waveg-
277 uide in the second episode coincided with a transfer of wave activity from the midlat-
278 itude to the subtropical waveguide.

279 We can envisage further fine tuning of the rolling zonalization procedure and waveg-
280 uide diagnostics. Instead of a threshold-based binary view of waveguide occurrence, more
281 nuanced information on waveguidability should be extractable from the background state.
282 Local wave activity (Huang & Nakamura, 2016, 2017; Ghinassi et al., 2018), computed
283 with respect to the longitudinally varying zonalized background state, presents a more
284 consistent measure of local waviness than the meridional wind. We intend to explore the
285 relationship between waveguidability properties of the rolling-zonalized background state
286 and wave packet propagation further in the future.

287 An atmospheric background state which is local in time and space and which is com-
288 putable from instantaneous data enables diagnostics to be applied in the full range of
289 lead times in forecast applications. Individual events can be investigated with regard to
290 the influence of teleconnection patterns or the potential of resonance along a circumglobal
291 waveguide. These are new and sought-after possibilities for current waveguidability re-
292 search (e.g. White et al., 2021; Riboldi et al., 2022).

293 Open Research

294 The code to reproduce the data analysis and all figures of this article is preserved
295 online (Polster, 2023). Procedures to compute the rolling zonalization are provided in
296 a Python package included in the associated code repository. ERA5 data (Hersbach et

297 al., 2023) was downloaded from the Copernicus Climate Change Service (C3S) Climate
 298 Data Store. The results contain modified Copernicus Climate Change Service informa-
 299 tion 2023. Neither the European Commission nor ECMWF is responsible for any use that
 300 may be made of the Copernicus information or data it contains.

301 Acknowledgments

302 We thank M. Riemer for valuable discussions about the rolling zonalization and its ap-
 303 plications. The research leading to these results has been done within the Transregional
 304 Collaborative Research Center SFB/TRR 165 “Waves to Weather” funded by the Ger-
 305 man Science Foundation (DFG).

306 References

- 307 Allen, D. R., & Nakamura, N. (2003). Tracer Equivalent Latitude: A Diagnos-
 308 tic Tool for Isentropic Transport Studies. *Journal of the Atmospheric Sciences*,
 309 *60*(2), 287–304. doi: 10.1175/1520-0469(2003)060<0287:TELADT>2.0.CO;2
- 310 Ambrizzi, T., Hoskins, B. J., & Hsu, H.-H. (1995). Rossby Wave Propagation
 311 and Teleconnection Patterns in the Austral Winter. *Journal of the Atmo-*
 312 *spheric Sciences*, *52*(21), 3661–3672. doi: 10.1175/1520-0469(1995)052<3661:
 313 *RWPATP>2.0.CO;2*
- 314 Borges, M. D., & Sardeshmukh, P. D. (1995). Barotropic Rossby Wave Dynam-
 315 ics of Zonally Varying Upper-Level Flows during Northern Winter. *Journal of*
 316 *the Atmospheric Sciences*, *52*(21), 3779–3796. doi: 10.1175/1520-0469(1995)
 317 *052<3779:BRWDOZ>2.0.CO;2*
- 318 Branstator, G. (1983). Horizontal Energy propagation in a Barotropic Atmosphere
 319 with Meridional and Zonal Structure. *Journal of Atmospheric Sciences*, *40*(7),
 320 1689 – 1708. (Place: Boston MA, USA Publisher: American Meteorological So-
 321 ciety) doi: 10.1175/1520-0469(1983)040<1689:HEPIAB>2.0.CO;2
- 322 Branstator, G. (2002, July). Circumglobal Teleconnections, the Jet Stream
 323 Waveguide, and the North Atlantic Oscillation. *Journal of Climate*,
 324 *15*(14), 1893–1910. (Publisher: American Meteorological Society) doi:
 325 10.1175/1520-0442(2002)015<1893:CTTJSW>2.0.CO;2
- 326 Branstator, G., & Teng, H. (2017). Tropospheric Waveguide Teleconnections and
 327 Their Seasonality. *Journal of the Atmospheric Sciences*, *74*(5), 1513–1532. doi:
 328 10.1175/JAS-D-16-0305.1
- 329 Bukenberger, M., Rüdīsühli, S., & Schemm, S. (2023). Jet stream dynamics from a
 330 PV gradient perspective: The method and its application to a km-scale sim-
 331 ulation. *Quarterly Journal of the Royal Meteorological Society*, qj.4513. doi:
 332 10.1002/qj.4513
- 333 Butchart, N., & Remsberg, E. E. (1986). The Area of the Stratospheric Po-
 334 lar Vortex as a Diagnostic for Tracer Transport on an Isentropic Sur-
 335 face. *Journal of Atmospheric Sciences*, *43*(13), 1319–1339. doi: 10.1175/
 336 1520-0469(1986)043<1319:TAOTSP>2.0.CO;2
- 337 Chang, E. K. M., Lee, S., & Swanson, K. L. (2002). Storm Track Dynamics. *Journal*
 338 *of Climate*, *15*(16), 2163 – 2183. doi: 10.1175/1520-0442(2002)015<02163:STD>
 339 *2.0.CO;2*
- 340 Chang, E. K. M., & Yu, D. B. (1999). Characteristics of Wave Packets in the Upper
 341 Troposphere. Part I: Northern Hemisphere Winter. *Journal of the Atmospheric*
 342 *Sciences*, *56*(11), 1708–1728. doi: 10.1175/1520-0469(1999)056<1708:COWPIT>
 343 *2.0.CO;2*
- 344 Davies, H. C. (2015). Weather chains during the 2013/2014 winter and their sig-
 345 nificance for seasonal prediction. *Nature Geoscience*, *8*(11), 833–837. doi: 10
 346 *.1038/ngeo2561*
- 347 Dritschel, D. G., & Scott, R. K. (2011). Jet sharpening by turbulent mixing. *Philo-*

- 348 *sophical Transactions of the Royal Society A: Mathematical, Physical and*
349 *Engineering Sciences*, 369(1937), 754–770. doi: 10.1098/rsta.2010.0306
- 350 Ghinassi, P., Baumgart, M., Teubler, F., Riemer, M., & Wirth, V. (2020). A
351 Budget Equation for the Amplitude of Rossby Wave Packets Based on Finite-
352 Amplitude Local Wave Activity. *Journal of the Atmospheric Sciences*, 77(1),
353 277–296. doi: 10.1175/JAS-D-19-0149.1
- 354 Ghinassi, P., Fragkoulidis, G., & Wirth, V. (2018). Local Finite-Amplitude Wave
355 Activity as a Diagnostic for Rossby Wave Packets. *Monthly Weather Review*,
356 146(12), 4099–4114. doi: 10.1175/MWR-D-18-0068.1
- 357 Harvey, B. J., Methven, J., & Ambaum, M. H. P. (2016). Rossby wave propaga-
358 tion on potential vorticity fronts with finite width. *Journal of Fluid Mechan-*
359 *ics*, 794, 775–797. doi: 10.1017/jfm.2016.180
- 360 Hersbach, H., Bell, B., Berrisford, P., Biavati, G., Horányi, A., Muñoz Sabater, J.,
361 ... others (2023). *ERA5 hourly data on pressure levels from 1940 to present*.
362 Copernicus Climate Change Service (C3S) Climate Data Store (CDS). doi:
363 10.24381/cds.bd0915c6
- 364 Hersbach, H., Bell, B., Berrisford, P., Hirahara, S., Horányi, A., Muñoz-Sabater, J.,
365 ... Thépaut, J. (2020). The ERA5 global reanalysis. *Quarterly Journal of the*
366 *Royal Meteorological Society*, 146(730), 1999–2049. doi: 10.1002/qj.3803
- 367 Hoskins, B. J. (2013). The potential for skill across the range of the seamless
368 weather-climate prediction problem: a stimulus for our science. *Quar-*
369 *terly Journal of the Royal Meteorological Society*, 139(672), 573–584. doi:
370 10.1002/qj.1991
- 371 Hoskins, B. J., & Ambrizzi, T. (1993, June). Rossby Wave Propagation on a Realis-
372 tic Longitudinally Varying Flow. *Journal of the Atmospheric Sciences*, 50(12),
373 1661–1671. (Publisher: American Meteorological Society) doi: 10.1175/1520-
374 -0469(1993)050<1661:RWPOAR>2.0.CO;2
- 375 Hoskins, B. J., & Karoly, D. J. (1981). The Steady Linear Response of a Spherical
376 Atmosphere to Thermal and Orographic Forcing. *Journal of the Atmospheric*
377 *Sciences*, 38(6), 1179–1196. doi: 10.1175/1520-0469(1981)038<1179:TSLROA>2
378 .0.CO;2
- 379 Hsu, H.-H., & Lin, S.-H. (1992). Global Teleconnections in the 250-mb Streamfunc-
380 tion Field during the Northern Hemisphere Winter. *Monthly Weather Review*,
381 120(7), 1169–1190. doi: 10.1175/1520-0493(1992)120<1169:GTITMS>2.0.CO;2
- 382 Huang, C. S. Y., & Nakamura, N. (2016). Local Finite-Amplitude Wave Activity as
383 a Diagnostic of Anomalous Weather Events. *Journal of the Atmospheric Sci-*
384 *ences*, 73(1), 211–229. doi: 10.1175/JAS-D-15-0194.1
- 385 Huang, C. S. Y., & Nakamura, N. (2017). Local wave activity budgets of the
386 wintertime Northern Hemisphere: Implication for the Pacific and Atlantic
387 storm tracks. *Geophysical Research Letters*, 44(11), 5673–5682. doi:
388 10.1002/2017GL073760
- 389 Karoly, D. J. (1983, March). Rossby wave propagation in a barotropic at-
390 mosphere. *Dynamics of Atmospheres and Oceans*, 7(2), 111–125. doi:
391 10.1016/0377-0265(83)90013-1
- 392 Kornhuber, K., Petoukhov, V., Petri, S., Rahmstorf, S., & Coumou, D. (2017). Ev-
393 idence for wave resonance as a key mechanism for generating high-amplitude
394 quasi-stationary waves in boreal summer. *Climate Dynamics*, 49(5-6), 1961–
395 1979. doi: 10.1007/s00382-016-3399-6
- 396 Luo, D., Luo, B., & Zhang, W. (2023). A Perspective on the Evolution of At-
397 mospheric Blocking Theories: From Eddy-Mean flow Interaction to Non-
398 linear Multiscale Interaction. *Advances in Atmospheric Sciences*. doi:
399 10.1007/s00376-022-2194-z
- 400 Maddison, J. W., Gray, S. L., Martínez-Alvarado, O., & Williams, K. D. (2019).
401 Upstream Cyclone Influence on the Predictability of Block Onsets over the
402 Euro-Atlantic Region. *Monthly Weather Review*, 147(4), 1277–1296. doi:

- 10.1175/MWR-D-18-0226.1
- 403
404 Manola, I., Selten, F., de Vries, H., & Hazeleger, W. (2013, September). “Wave-
405 uidability” of idealized jets. *Journal of Geophysical Research: Atmospheres*,
406 *118*(18), 10,432–10,440. doi: 10.1002/jgrd.50758
- 407 Martin, J. E. (2021). Recent Trends in the Waviness of the Northern Hemisphere
408 Wintertime Polar and Subtropical Jets. *Journal of Geophysical Research: At-
409 mospheres*, *126*(9). doi: 10.1029/2020JD033668
- 410 Martius, O., Schwierz, C., & Davies, H. C. (2006, January). A refined Hovmöller
411 diagram. *Tellus A: Dynamic Meteorology and Oceanography*, *58*(2), 221–226.
412 doi: 10.1111/j.1600-0870.2006.00172.x
- 413 Martius, O., Schwierz, C., & Davies, H. C. (2010, March). Tropopause-Level Wave-
414 guides. *Journal of the Atmospheric Sciences*, *67*(3), 866–879. doi: 10.1175/
415 2009JAS2995.1
- 416 Methven, J., & Berrisford, P. (2015). The slowly evolving background state of the
417 atmosphere. *Quarterly Journal of the Royal Meteorological Society*, *141*(691),
418 2237–2258. doi: 10.1002/qj.2518
- 419 Nakamura, N., & Huang, C. S. Y. (2018). Atmospheric blocking as a traffic jam in
420 the jet stream. *Science*, *361*(6397), 42–47. doi: 10.1126/science.aat0721
- 421 Nakamura, N., & Solomon, A. (2011). Finite-Amplitude Wave Activity and Mean
422 Flow Adjustments in the Atmospheric General Circulation. Part II: Analysis
423 in the Isentropic Coordinate. *Journal of the Atmospheric Sciences*, *68*(11),
424 2783–2799. doi: 10.1175/2011JAS3685.1
- 425 Nakamura, N., & Zhu, D. (2010). Finite-Amplitude Wave Activity and Diffusive
426 Flux of Potential Vorticity in Eddy–Mean Flow Interaction. *Journal of the At-
427 mospheric Sciences*, *67*(9), 2701–2716. doi: 10.1175/2010JAS3432.1
- 428 Petoukhov, V., Rahmstorf, S., Petri, S., & Schellnhuber, H. J. (2013). Quasiresonant
429 amplification of planetary waves and recent Northern Hemisphere weather ex-
430 tremes. *Proceedings of the National Academy of Sciences*, *110*(14), 5336–5341.
431 doi: 10.1073/pnas.1222000110
- 432 Polster, C. (2023). *wavestoweather/Rolling-Zonalization: v1.0*. Zenodo. Retrieved
433 2023-08-28, from <https://doi.org/10.5281/zenodo.8300732> doi: 10.5281/
434 zenodo.8300732
- 435 Polster, C., & Wirth, V. (2023). The Onset of a Blocking Event as a “Traffic Jam”:
436 Characterization with Ensemble Sensitivity Analysis. *Journal of the Atmo-
437 spheric Sciences*, *80*(7), 1681–1699. doi: 10.1175/JAS-D-21-0312.1
- 438 Riboldi, J., Rousi, E., D’Andrea, F., Rivière, G., & Lott, F. (2022). Circum-
439 global Rossby wave patterns during boreal winter highlighted by space–time
440 spectral analysis. *Weather and Climate Dynamics*, *3*(2), 449–469. doi:
441 10.5194/wcd-3-449-2022
- 442 Rousi, E., Kornhuber, K., Beobide-Arsuaga, G., Luo, F., & Coumou, D. (2022).
443 Accelerated western European heatwave trends linked to more-persistent
444 double jets over Eurasia. *Nature Communications*, *13*(1), 3851. doi:
445 10.1038/s41467-022-31432-y
- 446 Röthlisberger, M., Martius, O., & Wernli, H. (2016, January). An algorithm for
447 identifying the initiation of synoptic-scale Rossby waves on potential vorticity
448 waveguides: Initiation of Rossby Waves on PV Waveguides. *Quarterly Journal
449 of the Royal Meteorological Society*, *142*(695), 889–900. doi: 10.1002/qj.2690
- 450 Schwierz, C., Dirren, S., & Davies, H. C. (2004). Forced Waves on a Zonally Aligned
451 Jet Stream. *Journal of the Atmospheric Sciences*, *61*(1), 73–87. doi: 10.1175/
452 1520-0469(2004)061(0073:FWOAZA)2.0.CO;2
- 453 Spensberger, C., Spengler, T., & Li, C. (2017). Upper-Tropospheric Jet Axis Detec-
454 tion and Application to the Boreal Winter 2013/14. *Monthly Weather Review*,
455 *145*(6), 2363–2374. doi: 10.1175/MWR-D-16-0467.1
- 456 Teng, H., & Branstator, G. (2019, December). Amplification of Waveguide Telecon-
457 nections in the Boreal Summer. *Current Climate Change Reports*, *5*(4), 421–

- 458 432. doi: 10.1007/s40641-019-00150-x
- 459 White, R. H. (2019). Detecting waveguides for atmospheric planetary waves: con-
 460 nections to extreme weather events. In C. Chen, A. Charantonis, J. Runge,
 461 & J. Brajard (Eds.), *Proceedings of the 9th International Workshop on Cli-
 462 mate Informatics: CI2019 9 (No. NCAR/TN- 561+PROC)* (pp. 219–223).
 463 UCAR/NCAR. doi: 10.5065/Y82J-F154
- 464 White, R. H., Kornhuber, K., Martius, O., & Wirth, V. (2021, November). From
 465 Atmospheric Waves to Heatwaves: A Waveguide Perspective for Under-
 466 standing and Predicting Concurrent, Persistent and Extreme Extratropi-
 467 cal Weather. *Bulletin of the American Meteorological Society*, 1–35. doi:
 468 10.1175/BAMS-D-21-0170.1
- 469 Wirth, V. (2020, April). Waveguidability of idealized midlatitude jets and the lim-
 470 itations of ray tracing theory. *Weather and Climate Dynamics*, 1(1), 111–125.
 471 doi: 10.5194/wcd-1-111-2020
- 472 Wirth, V., & Polster, C. (2021, July). The Problem of Diagnosing Jet Waveguid-
 473 ability in the Presence of Large-Amplitude Eddies. *Journal of the Atmospheric
 474 Sciences*. doi: 10.1175/JAS-D-20-0292.1
- 475 Wirth, V., Riemer, M., Chang, E. K. M., & Martius, O. (2018). Rossby Wave
 476 Packets on the Midlatitude Waveguide—A Review. *Monthly Weather Review*,
 477 146(7), 1965–2001. doi: 10.1175/MWR-D-16-0483.1